BUTTERWORTH HEINEMANN

A simple model to evaluate direct contact heat transfer and flow characteristics in annular two-phase flow

Marco Fossa
Dipartimento di Termoenergetica e Condizionamento Ambientale (DITEC), Università Degli Studi di Genova, Genova, Italy

Calculations are performed to study the behavior of air–water mixtures in vertical flows employing a simple model for the description of mass, momentum, and energy transfer in annular gas–liquid flows. The model is applied to various flow conditions including thermal nonequilibrium and variable cross section ducts.

Theoretical results agree reasonably well with experimental data regarding well-known isothermal flows. A contribution is provided to the understanding of the two-phase mixtures interactions for gas–liquid internal heat transfer in two-phase, annular, nonisothermal flows.

Keywords: two-phase flow; dispersed annular flow; three components 1-D models; nonequilibrium flows; direct contact heat transfer

Introduction

Two-phase flows are encountered in a wide range of industrial applications, such as chemical plants, nuclear reactors, oil wells and pipelines, and evaporators and condensers (Kreith and Bohem 1988; Bergles et al. 1981). The configuration or flow pattern taken up by mixing gas and liquid streams depends upon the flow rates of the two phases, on the physical properties, and on pipe geometry. Annular flow is one of the most important flow patterns, because it occurs frequently in industrial equipment. This flow regime is characterized by the presence of a liquid film along the pipe wall and a gas core, containing dispersed droplets, flowing in the central part of the duct. Despite its apparent simplicity with respect to other flow regimes, the annular configuration is very complicated in detail, which is reflected in great uncertainties in the prediction of the performances of annular two-phase systems.

The interface of the film is covered by a complex system of waves, whose behavior is a governing feature. Such waves have different shapes and propagation velocities that depend upon such global flow parameters as mass flow rates and geometry. The system of waves increases the pressure gradient in the system and gives rise to entrained droplets. The droplets are continuously entrained and redeposited on the film; this process of mass interchange between the gas core and the film is a crucial aspect of annular flow. In adiabatic flows, droplet concentration, phase velocities, and film shape vary along the pipe until steady values, several hundred diameters downstream of the mixing section, are reached. Thus, in two-phase flows, the flow development occurs over much longer distances than in single-phase flow. These distances are often comparable with the common sizes of industrial equipment whose performances, consequently, are strongly influenced by "entrance effects."

Over the past 30 years, considerable work has been carried out in the direction of the phenomenological and theoretical characterization of the two-phase regimes and, in particular, of annular flow regime (Binder and Hanratty 1991; Ishii and Mishima 1989).

Nevertheless, research in this field is still intense and many studies and several conferences are devoted to this subject. In fact, many important questions await answers: one is related to developing flows structure and interactions, because only a few works investigated these problems extensively. Another crucial question concerns the physical modeling of two-phase flow, because universally accepted criteria do not exist. Different interpretations hold about droplet formation from wavy film and about the nature of wavy structure of the film itself. As a consequence, many correlations are available for the prediction of the main flow parameters (among these, film thickness, film flow rate, pressure gradient, mean droplet diameter), but sometimes different correlations involve different groups of physical quantities to describe the same flow parameter (Hewitt and Govan 1990; Andreussi 1983).

This work is an attempt to provide a tool to study the transfer processes occurring in two-phase annular flow by means of one-dimensional (1-D), three components, steady flow analysis of air–water mixtures in thermal nonequilibrium.

The model allows the calculation of temperature and velocity distributions of each component (i.e., gas, liquid film, liquid droplets) as well as other quantities such as mean film thickness, mean droplet diameter, pressure drop, and evaporation rate.

The proposed procedure consists in solving a system of 16 ordinary differential equations and related proper closure relations. The process allows the evaluation of the lengths needed to reach steady (or quasisteady) thermal and dynamic flow conditions.

The aim of this study is, then, to outline the limits and possibilities of the simple model presented by means of the comparison of the theoretical data with available experimental

Address reprint requests to Dr. Marco Fossa, Dipartimento di Termoenergetica e Condizionamento Ambientale (DITEC), University of Genova, Via All'Opera Pia 15A, (1) 16145 Genova, Italy.

Received 27 June 1994; accepted 10 April 1995

In. J. Heat and Fluid Flow 16: 272–279, 1995

655 Avenue of the Americas, New York, NY 10010

0142–727X/95/$10.00
SSDI 0142–727X(95)00027–N

results and give a contribution for an insight of heat transfer and flow phenomena that take place in annular gas–liquid flows.

Physical modeling and mathematical formulation

The formulation of the model is developed with reference to the annular dispersed flow regime in steady-state subsonic conditions, assuming, in each duct section, pressure uniformity and mean values of temperature and velocity for each one of the three components: gas, droplets, and liquid film. The gas and the liquid streams exchange heat, mass, and momentum through heat transfer, evaporation, and interfacial friction, respectively. The liquid film and the droplet swarm again exchange mass and energy by means of a net flux of droplets removed from and redeposited onto the film surface. The gas phase is then a mixture of dry air and water vapor described by the vapor content per unit mass of dry gas χ (humidity ratio), which changes along the duct because of liquid evaporation driven by temperature and pressure variations.

The model can account for variable flow sections (smooth-shaped nozzles and diffusers). In such a case, the validity of experimental correlations obtained with cylindrical pipes was extended to piecewise conical ones. Two liquid injection modes are considered; i.e., central nozzle or circumferential (porous) mixing device.

The thermophysical properties of the phases (among these: specific heat and enthalpy, density, thermal conductivity, surface tension, mass diffusivity, saturation pressure) are evaluated from local temperature and pressure values by means of least-square fitting functions of tabulated data in the temperature range (0–300)°C.

The conservation equations were applied to the three components flowing in the duct together with the constitutive equations and proper closure relationships. The complete set of equations used for developing the present work is for convenience reported in the Appendix.

Results and discussion

The analytical model described in the Appendix has been used for the couple air–water to simulate the vertical upward and downward annular flow. The main flow parameters have been calculated for a set of operating conditions including different liquid injection modes, flow rates, inlet temperatures, and pipe geometry.

Many experimental studies have been carried out with isothermal flows in vertical pipes. On the other hand, little information seems available about thermal nonequilibrium annular mixtures and two-phase flows in nozzles.

The results of the present theory have been compared with Gill et al. (1963) and Hewitt (1987) data for upward flows, while measurements of Okada and Fujita (1993) have been considered for downward flows. Hewitt's experiments were conducted with a circular pipe of 5 m length and 31.75 mm i.d. for fixed phase flow rates, 0.126 kg/s of water and 0.063 kg/s of air at room temperature. The resulting superficial phase velocities in the channel were around 40 m/s for the gas and 0.16 m/s for the liquid. Two forms of liquid injector were employed, a porous wall made of sintered bronze and a central jet injector of 4 mm i.d.

Notation

A	flow section, m^2
c	sound velocity, m/s
C	droplet concentration, kg/m^3
C_d	drag factor
c_p	specific heat at constant pressure, J/kgK
D	pipe diameter, m
D_i	injector diameter, m
D_p	Sauter mean droplet diameter, m
D_v	mass diffusivity, m^2/s
F	force per unit duct length, N/m
f	friction factor
g	acceleration of gravity, m/s^2
h	enthalpy, J/kg
h_c	convective heat transfer coefficient, W/m^2K
h_m	mass transfer coefficient, m/s
i	relative humidity, $i = \rho_v/\rho_s$
k	thermal conductivity, W/mK
K_d	deposition coefficient, m/s
L	length, m
$\dot{m}'$	mass flow rate per unit duct length, kg/s m
$\dot{m}$	mass flow rate, kg/s
N	number of droplets per unit volume, m^{-3}
Nu_d	droplet Nusselt number, $Nu_d = h_c D_p/k$
Nu_f	liquid film Nusselt number, $Nu_f = h_c D/k$
Pr	Prandtl number, $Pr = c_p \rho \nu/k$
p	pressure, Pa
p_s	vapor pressure at saturation, Pa
p_v	partial vapor pressure, Pa
q	heat flux per unit duct length, W/m
Re_g	gas Reynolds number, $Re_g = V_g D/\nu_g$
Re_d	droplet Reynolds number, $Re_d = (V_g - V_l)D_p/\nu_g$
S	interfacial area, m^2
Sh	Sherwood number, $Sh = h_m D/D_v$
Sc	Schmidt number, $Sc = \nu/D_v$
T	temperature, K
V	velocity, m/s
V_s	superficial velocity, $V_s = \dot{m}/(\rho A)$, m/s
We	Weber number, $We = \rho_g V_g^2 D/\sigma$

Greek

α	void fraction
δ	mean film thickness, m
ϑ	included angle
χ	humidity ratio
ν	kinematic viscosity, m^2/s
ρ	density, kg/m^3
σ	surface tension, N/m
τ	shear stress, N/m^2

Superscript

*	Critic

Subscripts

a	dry gas
c	gas core
e	entrained
f	liquid film
g	gas stream
hm	homogeneous mixture
i	interface, also at the injection
l	liquid droplet
s	smooth pipe, also at saturation
t	at the throat
v	vapor
w	wall

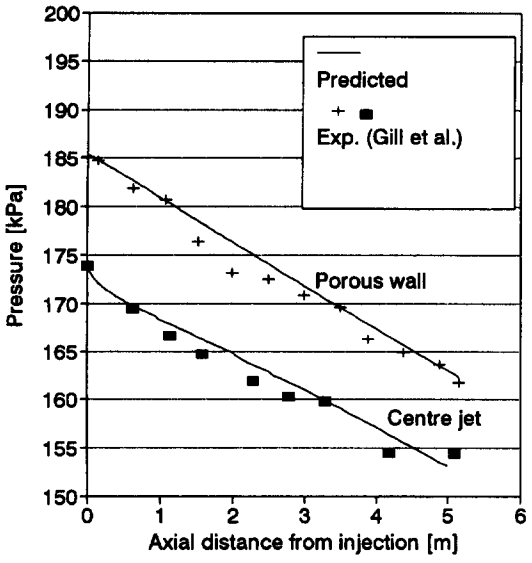

Figure 1 Calculated and measured (Gill et al. 1963) pressure profiles for two injection devices; $V_{sg}=40$ m/s, $V_{sl}=0.16$ m/s; pipe diameter 31.75 mm; upward flow

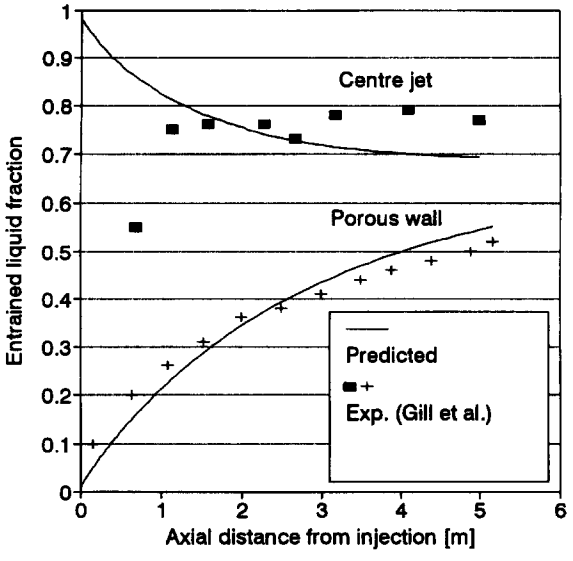

Figure 3 Calculated and measured (Gill et al. 1963) entrained liquid fraction profiles for two injection devices; $V_{sg}=40$ m/s, $V_{sl}=0.16$ m/s; pipe diameter 31.75 mm; upward flow

Figure 1 shows experimental and calculated pressure against the axial coordinate for the two different injection modes. The accordance is good: the maximum error on local pressure is about 5%, while the predicted outlet values, for both the liquid feed systems, practically coincide with the empirical data; furthermore, the calculated and experimental curves show similar trends, giving rise to mean pressure gradients in good agreement.

The mean film thickness and the entrained fraction are reported in Figures 2 and 3, respectively. The results of the simulations are satisfactory even if differences between measured and calculated data of the order of 30% exist all over the duct length. For this set of experimental data, the proposed model allows a reasonable prediction of the flow parameters, and it can account for the influence of the injection device on flow development.

In Okada and Fujita's (1993) experiments, the superficial gas velocity V_{sg} ranges from 20 to 90 m/s, and the liquid superficial velocity V_{sl} from 0.01 to 0.05 m/s. The measurements were conducted with a vertical pipe (i.d. 29.57 mm, 6 m long) in order to evaluate the film characteristics (mean, maximum, and minimum thickness) and the repartition of the liquid phase between droplets and film.

The simulations related to these tests were carried out for different flow conditions and liquid injectors. The results obtained show a systematic gap from experimental values in the direction of the overprediction of the mean film thickness and the liquid film fraction. In Figure 4, the calculated film thickness curves are reported together with the measured points for the upper and the lower liquid flow rate realized in Okada and Fujita (1993) and one gas flow rate. The trend is typical of all simulations; the error in the film properties estimation grows as the liquid flow rate reduces. In

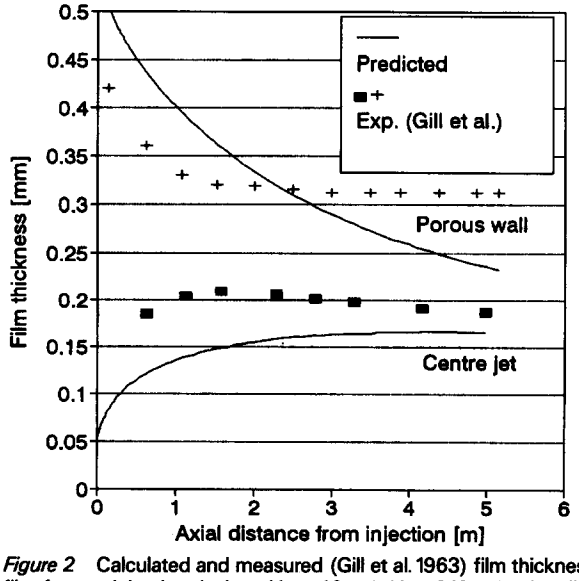

Figure 2 Calculated and measured (Gill et al. 1963) film thickness profiles for two injection devices; $V_{sg}=40$ m/s, $V_{sl}=0.16$ m/s; pipe diameter 31.75 mm; upward flow

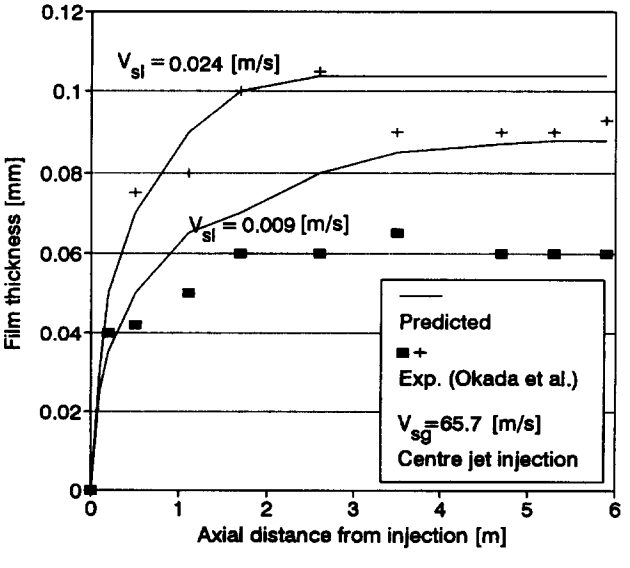

Figure 4 Calculated and measured (Okada and Fujita 1993) film thickness profiles for two different liquid flow rates (V_{sl} respectively 0.017 m/s and 0.009 m/s); $V_{sg}=65.7$ m/s; center jet injection; pipe diameter 29.57 mm; downward flow

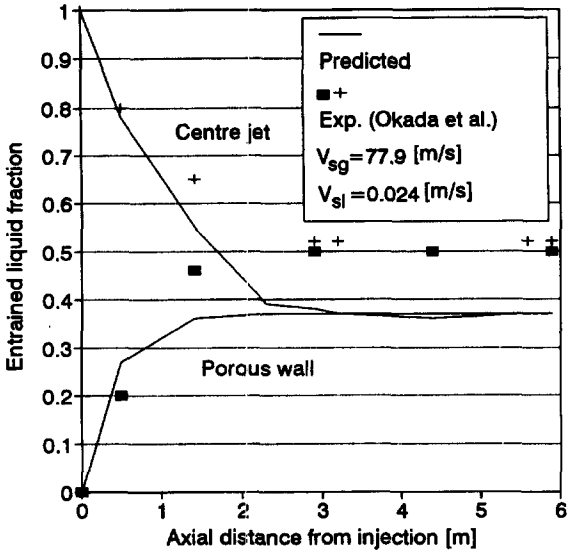

Figure 5 Calculated and measured (Okada and Fujita 1993) entrained liquid fraction profiles for two different injection devices; $V_{sl}=0.017$ m/s, $V_{sg}=77.9$ m/s; pipe diameter 29.57 mm; downward flow

Figure 5, data concerning the entrained liquid fraction are presented as an example for both porous and jet liquid injections ($V_{sl}=0.024$ m/s, $V_{sg}=77.9$ m/s). The calculated curves provide smaller values of the local and final entrained liquid fractions. Figure 6 summarizes the results of the simulations. It shows the entrained fraction at the outlet as a function of the gas flow rate (expressed in terms of V_{sg}) for two limit liquid flow rate conditions, $V_{sl}=0.014$ and $V_{sl}=0.024$ m/s. As already pointed out, these simulations give lower values of the final entrained liquid fraction. This evidence seems to denote some lack of accuracy in the correlations adopted to describe the dispersed phase formation and in the procedure that manages them. The discrepancies especially concern the simulation of downward flows (if compared with upward flows previsions), and the circumstance probably indicate

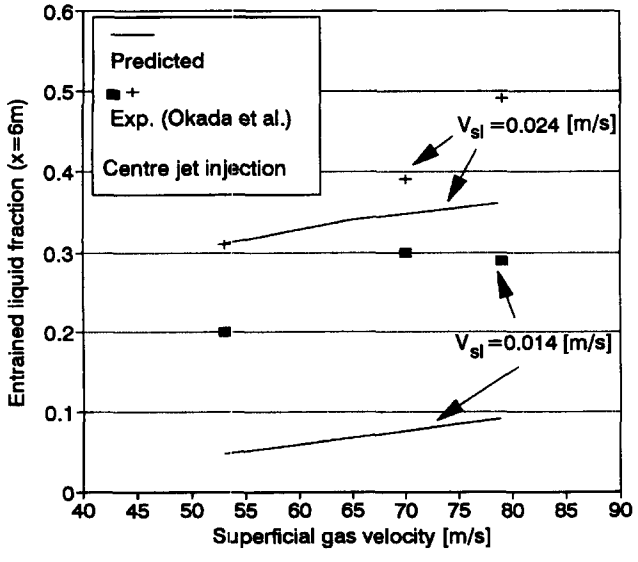

Figure 6 Predicted and measured (Okada and Fujita 1993) values of the entrained liquid fraction at the outlet as a function of the gas superficial velocity for two different liquid flow rates (V_{sl} respectively 0.024 m/s and 0.014 m/s); pipe diameter 29.57 mm; downward flow

the need of appropriate relationships to account for flow direction. Furthermore, the measurements show the existence of not negligible droplet flow rates in correspondence of film flow rates below the threshold values expected for the onset of entrainment.

As outlined before, another feature of the present model is to simulate nonisothermal flows either in straight pipes or variable cross section ducts. Because the scientific literature does not cover this topic from the experimental point of view (except for some preliminary studies carried out by the author, Fossa et al. 1993), a comparison with measured data in this case is not possible. As an example of the code capability to simulate this kind of flows, two ducts have been considered, 1 m long, with circular cross section and outlet diameter of 0.066 m. One differs from the other because of the presence of a converging nozzle (0.16 m long, included angle 8°) constituting its inlet stretch. Air ($\dot{m}_g=0.23$ kg/s) and water ($\dot{m}_l=0.077$ kg/s) are fed at different temperature ($T_g=295$ K, $T_l=370$ K) using a central liquid injection; the resulting superficial velocities are $V_{sg}=20$ m/s, $V_{sl}=0.022$ m/s. Finally two different injection nozzles giving rise to initial droplet diameter D_{pi} of 100 μm and 200 μm have been considered. The model of Azzopardi (1984) was adopted to account for the effects of the geometrical singularity on the flow parameters (see Appendix).

The variations of the main flow parameters (temperature, velocity, pressure) along the pipe are reported in the Figures 7a–c ($D_{pi}=100$ μm) and 8a–c ($D_{pi}=200$ μm). Dotted curves represent the converging pipe, and continuous curves refer to the constant cross section pipe. Dotted and continuous profiles are similar and attain the same asymptotic values. Only the pressure trends show a different behavior caused by the gas acceleration in the initial part of the channel. The temperature profiles are strongly influenced by droplet diameter, which controls the exchange surface between the liquid and the gas; the result, as could be expected, is a more effective heat transfer related to the smaller droplet diameter. This circumstance also affects the liquid film temperature profile by means of the process of "cold" droplet deposition.

It is worthwhile to note, furthermore, the role of the pressure drop on liquid change of phase; whereas, the pressure gradients are higher there (the case of the convergent pipe), a more intense evaporation (which contributes to the liquid temperature lowering) occurs.

Conclusions

A 1-D, three components, model has been proposed for the evaluation of heat transfer and flow characteristics of two-phase annular flow. The present method, able to account for deposition and entrainment processes as well as evaporation and heat transfer between cocurrent air and water flows, has been proved to be valid.

As a matter of fact, the comparison between the experimental data concerning upward and downward isothermal mixtures and numerical previsions shows a quite satisfactory agreement. The measured pressure profiles of Gill et al. (1963) are well reproduced by their theoretical counterparts, while discrepancies were found for the comparison with measured parameters in downward flows. Nevertheless, the extensive comparison with downflow measurements allows us to assert that the model is mainly reliable to predict the behavior of high velocity downward flows.

The heat transfer between the phases has been simulated for straight pipes and variable cross section ducts, and the role of droplet diameter and pressure gradient has been outlined. To check the predicted flow thermal history, further studies on the evaluation of the temperature distributions inside two phase mixtures are desirable.

The development of the model, finally, requires the comparison of different closure relationships with several sets of data and the

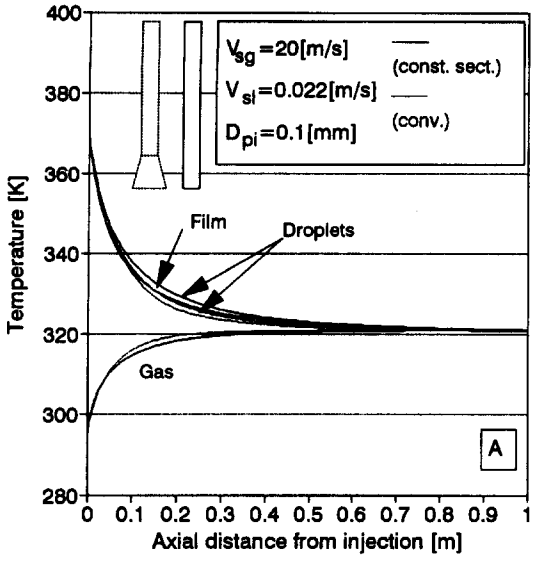

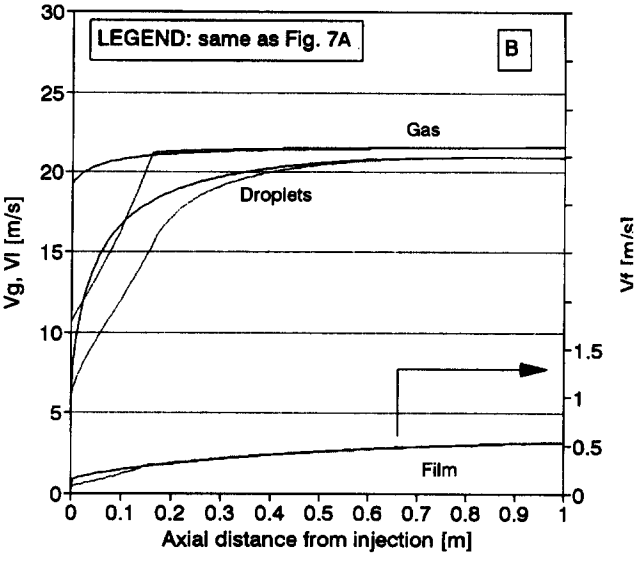

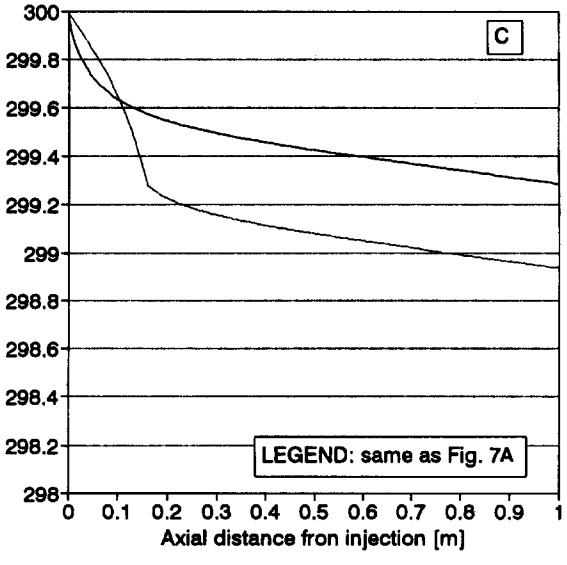

Figure 7 Predicted profiles of pressure (A), velocity (B), and temperature (C) in a nonisothermal upward flow. Continuous curves: straight pipe. Dotted curves: convergent-straight pipe. $V_{sg}=20$ m/s, $V_{sl}=0.022$ m/s. Droplet diameter at the injection 100 μm

adoption of appropriate correlations for accounting of phenomena related to flow direction, as these preliminary results seem to suggest.

Appendix

The conservation equations (mass, momentum, and energy) are written in the usual form for each of the three components moving upward in a pipe of cross section (A_c+A_f); the quantities flow rate $(\dot{m}')$, force F, and heat flux q are defined per unit duct length.

$$\frac{d}{dx}(\rho_g V_g \alpha_c A) - \dot{m}_a \frac{d\chi}{dx} = 0 \qquad (A1a)$$

$$\frac{d}{dx}[\rho_l V_l (1-\alpha_c) A_c] - \dot{m}'_e + \dot{m}'_d + \dot{m}'_{vl} = 0 \qquad (A1b)$$

$$\frac{d}{dx}(\rho_f V_f A_f) + \dot{m}'_e - \dot{m}'_d + \dot{m}_{vf} = 0 \qquad (A1c)$$

$$\dot{m}_a \frac{d\chi}{dx} = \dot{m}'_{vf} + \dot{m}'_{vl} \qquad (A2)$$

$$\rho_g V_g \alpha_c A_c \frac{d}{dx}(V_g) + \dot{m}'_{vl}(V_g - V_{vl}) + \dot{m}'_{vf}(V_g - V_{vf}) = -\rho_g \alpha_c A g - F_d - F_i - \alpha_c A \frac{dp}{dx} \qquad (A3a)$$

$$\rho_l V_l (1-\alpha_c) A_c \frac{d}{dx}(V_l) + \dot{m}'_e (V_l - V_f) + \dot{m}'_{vl}(V_{vl} - V_l) = -(1-\alpha_c) A_c \left(\frac{dp}{dx} + \rho_l g\right) + F_d \qquad (A3b)$$

$$\rho_f V_f A_f \frac{d}{dx}(V_f) + \dot{m}'_d (V_f - V_l) + \dot{m}'_{vf}(V_{vf} - V_f) = -A_f \frac{dp}{dx} - \rho_f A_f g + F_i - F_w \qquad (A3c)$$

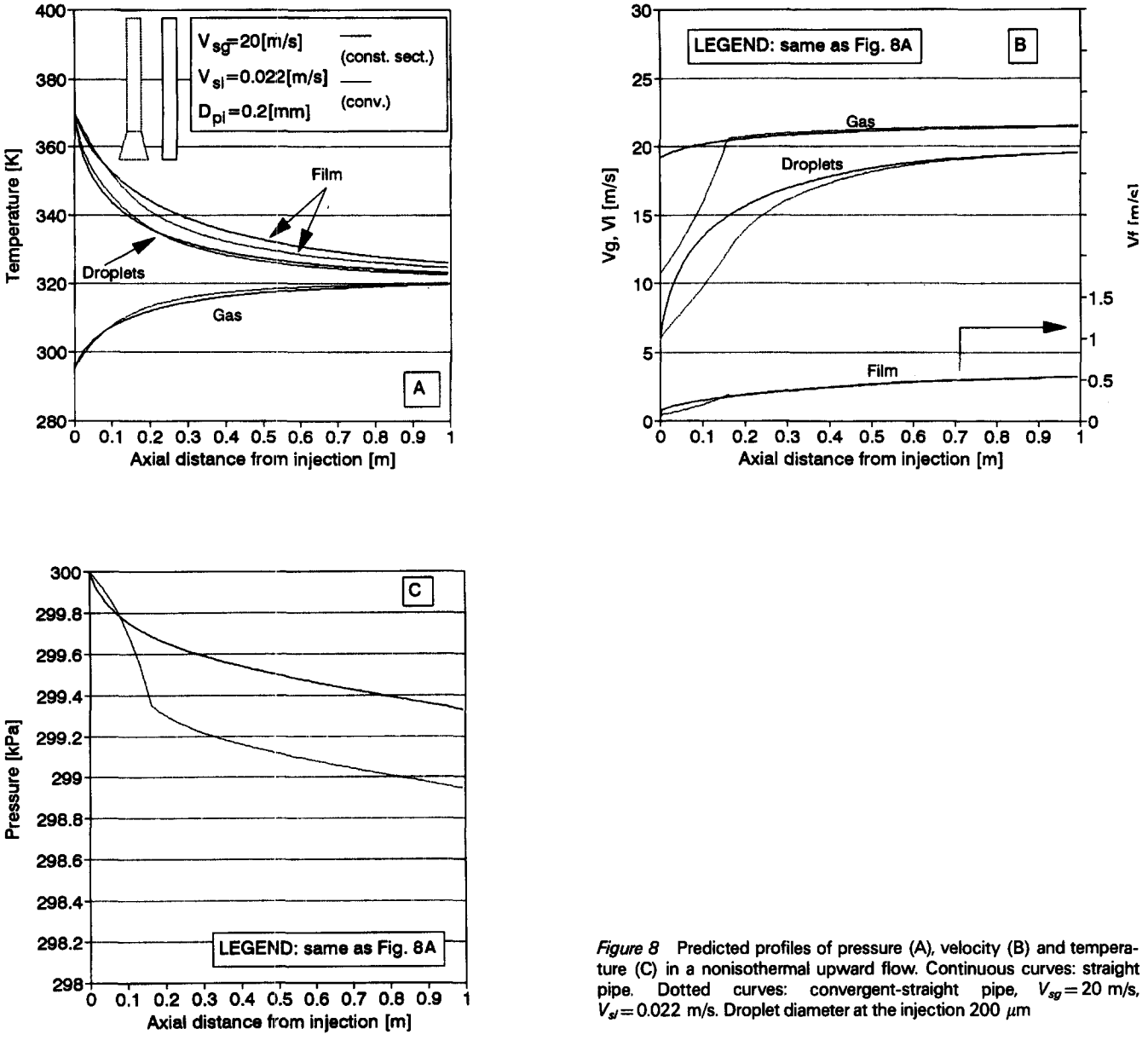

Figure 8 Predicted profiles of pressure (A), velocity (B) and temperature (C) in a nonisothermal upward flow. Continuous curves: straight pipe. Dotted curves: convergent-straight pipe, $V_{sg}=20$ m/s, $V_{sl}=0.022$ m/s. Droplet diameter at the injection 200 μm

$$\rho_g \alpha_c A_c V_g \frac{d}{dx}(h_g + gx + V_g^2/2) + \dot{m}'_{vl}[h_g - h_{vl} + (V_g^2 - V_{vl}^2)/2] + \dot{m}_{vf}[h_g - h_{vf} + (V_g^2 - V_{vf}^2)/2] = q_l + q_f - F_l V_l - F_i V_f \quad (A4a)$$

$$\rho_l(1-\alpha_c)A_c V_l \frac{d}{dx}(h_l + gx + V_l^2/2) - \dot{m}'_{vl}[h_l - h_{vl} + (V_l^2 - V_{vl}^2)/2] + \dot{m}'_e[h_l - h_f + (V_l^2 - V_f^2)/2] = -q_l + F_i V_l \quad (A4b)$$

$$\rho_f A_f V_f \frac{d}{dx}(h_f + gx + V_f^2/2) + \dot{m}'_{vf}[h_{vf} - h_f + (V_{vf}^2 - V_f^2)/2] + \dot{m}'_d[h_f - h_l + (V_f^2 - V_l^2)/2] = F_i V_f - (q_{ext} + q_l) \quad (A4c)$$

The terms in the energy equations include mass transfer caused by phase change as well as entrainment and deposition; it has been supposed that the heat transfer q_{ext} between the system and the surroundings (if present) involves only the film. Equation A2 arises from the definition of humidity ratio; here $\dot{m}_a$ is the dry gas flow rate, constant along the pipe.

Furthermore, the vapor phase is assumed to enter the gas phase with velocity V_v and enthalpy h_v: the first has been supposed equal to the arithmetic mean of liquid (film or droplets) and gas velocities, and the second is assumed equal to the saturation enthalpy of the vapor at the liquid temperature.

To complete the system of Equations (A1–A4), it is necessary to introduce the constitutive equations of the two phases. The gas phase is modeled as an ideal gas mixture whose enthalpy is a function of the temperature and the humidity ratio. Enthalpy variations of the liquid phase are supposed to be driven only by temperature variations through the specific heat parameter.

To solve the set of equations for given liquid and gas flow rate, stream properties, and pipe geometry, several closure relations are needed. Such relations define the dynamics of heat, mass, and momentum transfer.

Here is a short summary of the correlations adopted. The

friction force between the gaseous stream and the liquid film is defined as follows:

$$F_i = 0.5 f_i \rho_g (V_g - V_f)|V_g - V_f| \pi (D - 2\delta) \quad (A5)$$

where f_i is the interfacial friction coefficient. This last is provided, as suggested by several authors, by means of the single-phase, smooth pipe friction factor f_s multiplied by an assigned function of the mean liquid film thickness δ that accounts for the roughening of the film by means of the waves. In this work, the correlation of Whalley and Hewitt (1978) was adopted:

$$f_i = f_s[1 + 24(\rho_l/\rho_g)^{0.5}\delta/D] \quad (A6)$$

The wall friction force acting on the liquid film is evaluated from single phase friction factor correlations based on liquid film Reynolds number.

The drag force between the droplets and the gas has been expressed as follows:

$$F_d = 0.5\, C_d \pi \frac{D_p^2}{4} \rho_g (V_g - V_l)|V_g - V_l| NA \quad (A7)$$

where C_d is the drag coefficient of a nonrotating spherical body (Claviere 1978) and N is the number of droplets per unit volume (which depends upon the gas core void fraction α_c and on mean droplet diameter D_p).

The mean droplet diameter is a basic parameter in all the exchange processes occurring between the phases. Two correlations are used to estimate it. The first correlation gives the Sauter mean diameter D_{pi} of a swarm of droplets generated by an injector of given orifice diameter D_i (Nukiyama and Tanasawa 1938). The second one (Azzopardi et al. 1979) provides the size D_{pf} of the entrained particles from atomizing film waves.

$$D_{pi} = \frac{0.585\sqrt{\sigma/\rho_l}}{V_g - V_l} + 53.2\left(\frac{\mu_l}{\sqrt{\sigma/\rho_l}}\right)^{0.45}(V_{sg} - V_{sl})^{1.5} \quad (A8)$$

$$\frac{D_{pf}}{D} = 1.91\frac{\mathrm{Re}_g^{0.11}}{\mathrm{We}^{0.6}}\left(\frac{\rho_g}{\rho_l}\right)^{0.6} + 0.4\frac{V_l}{V_g}(1 - \alpha) \quad (A9)$$

$$\mathrm{We} = \frac{\rho_g V_g^2 D}{\sigma}; \qquad \mathrm{Re}_g = \frac{V_g D}{\nu_g} \quad (A10)$$

The actual mean droplet diameter D_p is then evaluated according to the following procedure. At the inlet, if an axial injector is present, D_p is equal to D_{pi}. At each location x in the flow direction, depending upon the local mass fluxes $\dot{m}_e$ and $\dot{m}_d$, new droplets of $D_{pf}(x)$ diameter are entrained, and some droplets of $D_p(x)$ diameter redeposit back onto the film.

Therefore, at the following position, the mean droplet diameter $D_p(x+\Delta x)$ is obtained as Sauter mean of the droplet population formed by the two families of different diameter, that is, by calculating the ratio between overall droplet volume and overall droplet area.

Finally, the droplet mean diameter is checked according to the criterion (Hinze 1955) that states the existence of a critical diameter, as a function of Weber number, above which the forces acting on the particle cause the droplet breakup.

To predict the local mean droplet diameter, it is necessary to evaluate the mass fluxes of entrainment and deposition. The mechanism of droplet entrainment is complex; as reported by several authors (James et al. 1980; Azzopardi 1983), it is related to the onset of disturbance waves on the film surface, which seems to depend basically upon liquid film flow rate. The practical consequence is the existence of a limiting value of the film flow rate below which no entrainment occurs. According to Hewitt and Govan (1990) the critical film flow rate is given by the following empirical relationship:

$$\mathrm{Re}_f^* = \frac{V_{sf}^* D}{\nu_f} = e^{(5.8504 + 0.4249(\mu_g/\mu_l)\sqrt{\rho_l/\rho_g})} \quad (A12)$$

As suggested by the same authors, the mass fluxes $\dot{m}_e$ and $\dot{m}_d$ may be calculated from the following correlations involving droplet mass concentration C:

$$\dot{m}_d'/(\pi D) = K_d C \quad (A13)$$

$$K_d\sqrt{\rho_g D/\sigma} = 0.18 \qquad C/\rho_g < 0.3 \quad (A14)$$

$$K_d\sqrt{\rho_g D/\sigma} = 0.083(C/\rho_g)^{-0.65} \qquad C/\rho_g > 0.3 \quad (A15)$$

$$\dot{m}_e'/(V_{sg}\rho_g \pi D) = 5.75 \times 10^{-5}\left[\rho_l (V_{sf} - V_{sf}^*)^2 \frac{D\rho_l}{\sigma\rho_g^2}\right]^{0.316} \qquad V_{sf} > V_{sf}^* \quad (A16)$$

When a geometrical discontinuity exists, further correlations are needed to describe the evolution of the liquid interface. Azzopardi (1984) has considered the effects of conical constrictions (included angles between 18 and 90°) on vertical annular flow parameters. The experiments carried out show that the presence of the singularity causes the film flow rate to decrease: the wider is the included angle ϑ, the higher is the extra entrainment $\dot{m}_{et}$ that occurs at the start of the constriction throat. Azzopardi (1984) suggests that the ratio of liquid entrained to liquid remaining in the film is proportional to the tangent of the convergence half angle according to the relationship:

$$\dot{m}_{et} = \frac{\tan(\theta/2)}{1 + \tan(\theta/2)}(\dot{m}_f) \quad (A17)$$

To evaluate the convective heat transfer q_l between dispersed liquid and gas, the Nusselt number referred to the droplet diameter has been expressed by the correlation of Ranz and Marshall (1952):

$$\mathrm{Nu}_d = 2.0 + 0.6\,\mathrm{Re}_d^{1/2}\mathrm{Pr}^{1/3} \quad (A18)$$

The heat transfer between the gas and the liquid film has been associated to single-phase heat transfer in rough pipes, because no direct information seems to be available. Thus, the thermal exchange has been described by the correlation of Petukhov (1970):

$$\mathrm{Nu}_f = \frac{(f_i/2)\,\mathrm{Re}\,\mathrm{Pr}}{1.07 + 12.7(f_i/2)^{0.5}(\mathrm{Pr}^{2/3} - 1)} \quad (A19)$$

where f_i is the friction factor coefficient calculated from Equation A6.

The evaporation rate has been introduced on the basis of the heat–mass transfer analogy, which assumes the same Colburn numbers for the two transfer processes, so that:

$$\frac{\mathrm{Nu}}{\mathrm{Re}\,\mathrm{Pr}^{0.33}} = \frac{\mathrm{Sh}}{\mathrm{Re}\,\mathrm{Sc}^{0.33}} \quad (A20)$$

The mass transfer rate $\dot{m}_v$ thus results in the following:

$$\dot{m}_v = h_m S\,(\rho_{vs} - \rho_v)\,F(i) \quad (A21)$$

where h_m is the mass transfer coefficient; S the interfacial area; ρ_{vs} saturated vapor density at the liquid temperature; ρ_v the vapor density in the gas stream; and $F(i)$ is a trigger function of the gas relative humidity i, which inhibits the phase change when the gas reaches saturation conditions or when the vapor content goes to zero.

The above formulation of the physical problem yields a set of 16 first-order differential equations, which have been solved numerically with a Runge–Kutta Fehlberg method to get the development of the thermal and fluid dynamic characteristics of the two-phase flow along the streamwise x direction.

Two last considerations concern the existence of an annular flow pattern in upward flows and subsonic conditions. According to Turner et al. (1969), the first constraint is satisfied when:

$$\frac{V_{sg}\rho_g^{1/2}}{[\sigma g(\rho_l - \rho_g)]^{1/4}} \geq 3.1 \qquad (A22)$$

that is, for assigned pipe geometry and fluids, when the gas flow rate exceeds a certain value.

Subsonic flow condition may be controlled according to a theoretical equation that gives the critical flow velocity of a homogeneous gas–liquid mixture:

$$c_{hm}^2 = \left(\frac{p/\rho_l}{\alpha(1-\alpha)}\right) \qquad (A23)$$

A comparison with experimental data (Lemmonier and Selmer-Olsen 1992), suggests a conservative behavior of criterion (A23).

References

Andreussi, P. 1983. Droplet transfer in two phase annular flow. *Int. J. Multiphase Flow*, **9**, 697–713

Azzopardi, B. J., Freeman, G. and King, D. J. 1979. Drop sizes and deposition in annular two-phase flow. *UKAEA Rep. AERE-R 9634*

Azzopardi, B. J. 1983. Mechanism of entrainment in annular two phase flow. *UKAEA Rep. AERE-R11068*

Azzopardi, B. J. 1984. Annular Two Phase Flow in Constricted Tubes. *UKAEA Nat. Heat Transfer Conf.* Leeds, England

Bergles, A. E., Collier, J. G., Delhaye, J. M., Hewitt, G. F. and Mayinger, F. 1981. *Two-Phase Flow and Heat Transfer in the Power and Process Industries*. Hemisphere, Bristol, PA

Binder, J. L. and Hanratty, T. J. 1991. A diffusion model for droplet deposition in gas/liquid flows. *Int. J. Multiphase Flow*, **17**, 1–11

Claverie, J. 1978. Coefficient de trainee d'une sphere. *EDF DER, Dep. Machine*, HO 062 III.1.1

Fossa, M., Pisoni, C. and Tagliafico, L. A. 1993. Indagine sperimentale sui processi di scambio termico liquido gas in efflussi ascendenti in regime anulare. *Proc. 11th Nat. Heat Transfer Conf.* Milan

Gill, L. E., Hewitt, G. F., Hitchon, J. W. and Lacey, P. M. C. 1963. Sampling probe studies on the gas core in annular two-phase flow—I (The effect of length on phase and velocity distribution). *Chem. Eng. Science*, **18**, 525–535

Hewitt, G. F. 1987. Developing annular flow. In *Multiphase Science and Technology*, Hemisphere, Bristol, PA

Hewitt, G. F. and Govan, A. H. 1990. Phenomenological modeling of non-equilibrium flows with phase change. *Int. J. Heat Mass Transfer*, **33**, 229–242

Hinze, J. O. 1955. Fundamentals of the hydrodynamic mechanism of splitting in dispersion processes. *AIChE J.*, **1**, 289

Ishii, M. and Mishima, K. 1989. Droplet entrainment in annular two-phase flow, *Int. J. Multiphase Flow*, **32**, 1835–1845

James, P. W., Whalley, P. B. and Hewitt, G. F. 1980. Droplet motion in two phase flow. *Int. Meeting on Nuclear Reactor Therm. Hydraul.*, Saratoga Springs, NY

Kreith, F. and Bohem R. F. 1988. *Direct Contact Heat Transfer*. Hemisphere, Bristol, PA

Lemonnier, H. and Selmer-Olsen, S. 1992. Experimental investigation and physical modeling of two-phase two-component flow in a converging–diverging nozzle. *Int. J. Multiphase Flow*, **1**, 1–20

Nukiyama, S. and Tanasawa, I. 1938. *Trans. Soc. Mech. Eng. Jpn*, **4**, 86

Okada, O. and Fujita, H. 1993. Behavior of liquid films and droplets in the non-equilibrium region of a downward annular mist flow (comparison of porous and central nozzle mixing methods). *Int. J. Multiphase Flow*, **19**, 79–89

Petukhov, B. S. 1970. Heat transfer and friction in turbulent pipe flow with variable physical properties. In *Advances in Heat Transfer*, Academic, New York

Ranz, W. and Marshall, W. Jr. 1952. Evaporation from drops. *Chem. Eng. Prog.* **48**, 141–146

Turner, R. G., Hubbard, M. G. and Dukler, A. E. 1969. Analysis and prediction of minimum flow rate for the continuous removal of liquid from gas wells. *J. Petroleum Technol.* **21**, 1475

Whalley, P. B. and Hewitt, G. F. 1978. The correlation of liquid entrainment fraction and entrainment rate in annular two-phase flow. *AERE-R9187*